J. Chem. Sci. (2018) 130:123
https://doi.org/10.1007/s12039-018-1514-4

REGULAR ARTICLE

Kinetics and mechanistic study of the reduction of Mn^{III} by oxalate in Salophen scaffold: relevance to oxalate oxidase

PRIYAMBADA JENA[a], ACHYUTA N ACHARYA[a,*], V RAO MUNDLAPATI[b], ANADI C DASH[c,*] and HIMANSU S BISWAL[b,*]

[a]Department of Chemistry, College of Engineering and Technology, Bhubaneswar 751 029, India
[b]School of Chemical Sciences, National Institute of Science Education and Research (NISER), Bhimpur-Padanpur PO, Via-Jatni, Khurda, Bhubaneswar 752 050, India
[c]Department of Chemistry, Utkal University, Bhubaneswar 751 004, India
E-mail: aacharya@cet.edu.in; acdash41@gmail.com; himansu@niser.ac.in

MS received 16 May 2018; revised 24 June 2018; accepted 30 June 2018; published online 21 August 2018

Abstract. The *trans*-Mn^{III}(Salophen)$(OH_2)_2^+$ and bioxalate (HOX^-) in aqueous medium equilibrate rapidly to *trans*-Mn^{III}(Salophen)(OH_2)(HOX) followed by the acid dissociation equilibrium to the (aqua) mono oxalato complex. The slow redox reactions of *trans*-Mn^{III}(Salophen)$(OH_2)(HOX/OX)^{0/-}$ with H_2OX, HOX^-,OX^{2-} obey second order kinetics satisfying 2:1 stoichiometry ($[Mn^{III}]_T/[OX]_T = 2/1$). The products are Mn^{II} and CO_2. Acrylamide monomer has no effect on the rate constant and the reaction does not induce its polymerization. The rate and activation parameters for the various rate limiting paths are reported. The intramolecular reduction of Mn^{III} by the coordinated HOX^- and OX^{2-} in *trans*-Mn^{III}(Salophen)$(OH_2)(HOX/OX)^{0/-}$ could not be detected. Contrary to our expectation, it is observed that H_2OX is a better reducing agent than HOX^- for *trans*-Mn^{III}(Salophen)(OH_2)(HOX), the slowest being the redox reaction of OX^{2-} with *trans*-Mn^{III}(Salophen)$(OH_2)(OX)^-$. The molecular modelling by DFT depicts the structural *trans* effect in the oxalato complexes, it being maximum for *trans*-Mn^{III}(Salophen)$(OH_2)(OX)^-$. The observed sequence of the redox activity of the oxalato complexes reflects the potential role of non-covalent interaction *i.e.* H-bonding, governing the proton controlled electron transfer process (*PCET*). The Mn^{III}(Salophen/Salen) complexes may turn out to be good substitute candidates for Oxalo Oxidase (OXO) enzyme in alleviating the oxalate overload in plants and animal biochemistry.

Keywords. Kinetics; Mn^{III}(Salophen); oxalate; oxidation; oxalo oxidase.

1. Introduction

Previously we have reported the redox reactions of $Mn^{III}(Salen)^+$ by glyoxylate[1] and oxalate.[2] The redox process involves fast pre-equilibrium of the glyoxalate and oxalate species followed by slow electron transfer reactions between Mn^{III}(Salen)X (X = glyoxylate, HOX^-, OX^{2-}) and the corresponding acids, and their anions. It turned out that the binding of ligand X to Mn^{III} centre considerably stabilized Mn^{III} centre for intramolecular electron transfer in Mn^{III}(Salen)X. This is generally referred to as stabilization of metal oxidation state by ligand binding. Besides we found that in both cases (i.e. glyoxylate and oxalate oxidation) the acids are better reductants than their mono anions (and also dianion for oxalic acid). This is an unexpected result considering the electron donor properties of the acid molecules and their conjugate bases. However, the involvement of proton mediation in the redox process was believed to explain this reverse trend of reactivities and proton-coupled electron transfer process (PCET) was suggested. In such a situation, we believe that there is the possibility of hydrogen bonding of oxalic and glyoxylic acid molecules with the weakly basic coordinated phenoxide of Mn^{III}(Salen) which favoured the PCET process. Attempts were made to shed light on these aspects by molecular modelling at DFT level

*For correspondence
This work is dedicated to Late Professor Rabindra Kumar Nanda (ex-Professor & Head of the Department of Chemistry, Utkal University, Bhubaneswar).

Electronic supplementary material: The online version of this article (https://doi.org/10.1007/s12039-018-1514-4) contains supplementary material, which is available to authorized users.

with some degree of success. But this warrants further studies. What will be the consequence of such redox reactions when the salen moiety is manipulated? One of such studies is presented herein using Mn^{III}(Salophen)$^+$ (H_2salophen = *N*,*N*′-bis(salicylidene) 1,2-diamino benzene) as oxidant and oxalate as a reductant. The salophen motif provides rigidity to the structure of the Mn^{III} complex maintaining co-planarity of the donor sites. We focus our attention on the following aspects: (i) How do the structure and electronic property of the salen motif, due to the changes made in the central part of the di-imine skeleton, influence complex forming ability of Mn^{III} with oxalate species? (ii) how is the intramolecular electron transfer processes affected? (iii) how is the proton controlled electron transfer process between Mn^{III} and HOX^-/H_2OX mediated by this structural variation of the manganese complex? Moreover, PCET is a fundamental process involved in many chemical reactions and continues to be an active area of research.[3]

There is also another dimension to our research, i.e. to find a suitable substitute for the enzyme Oxalate Oxidase (OXO; E.C.1.2.3.4) which is widespread in nature particularly in plant tissues,[4] fungi[5] and bacteria[6] and functions as a catalyst for oxidation of oxalate, the metabolic by-product. The humans and other animals being deprived of this enzyme in their bio-system are seriously at risk of oxalate overload due to metabolic failure. This is one of the causes of kidney stones and renal failure, ultimately resulting in a threat to life. Can Mn^{III}(Salen/Salophen) be a suitable alternative for taking care of oxalate overload, be it in plants or animal kingdom? Not only the study of the mechanism of oxidation of oxalate is important, it is this aspect which encouraged us to undertake the present study in sequence to our earlier ones.

2. Experimental

2.1 *Materials and reagents*

The tetradentate Schiff base ligand H_2salophen was synthesized by condensing ortho-phenylenediamine with salicylaldehyde in 1:2 mole proportion in methanol. The solid product was purified by recrystallization from methanol, air dried and stored over silica gel in a desiccator avoiding exposure to moisture and light.

2.1a $[Mn^{III}(Salophen)(OH_2)_2]ClO_4, H_2O$: For the synthesis of the Mn^{III}complex,[7] manganese(III) acetate dihydrate (4 mmol) and the Schiff base (H_2salophen) (4 mmol) were mixed in ~250 cm^3 methanol to which 6 mmol of $LiClO_4$ in 80 cm^3 of water was added. The solution was evaporated to ~ 40 cm^3 and then left to cool to room temperature. The resulting product (black crystals) was filtered under suction using a glass sintered funnel and recrystallized from methanol–water (50% v/v). The product was air-dried and stored over silica gel in a desiccator being protected from light and moisture. It may be noted that Yuan *et al*.,[7] mentioned the composition of this complex as Mn^{III}(Salophen)(OH_2) ClO_4.

Caution *! Perchlorate salt of the Mn^{III} complex may be potentially hazardous. As such only small amounts may be prepared and handled with care.*

Anal. Calcd. For $[Mn^{III}(Salophen)(OH_2)_2]ClO_4,H_2O$ (F. wt. 522.8): C, 45.9; N, 5.36; H, 3.85%. Found: C, 45.4; N, 5.29; H, 3.30%. ESI-MS from aqueous medium (Figure S1a, Supplementary Information) m/z^+; 369.044 (obs), 369.288 (calcd. for Mn(Salophen)), $(m/z^+)+1$; 370.046 (obs); m/z^+: 837.033 (obs.), 837.068 {calcd. for {[Mn(Salophen)OCl(O_2) OMn(Salophen)]-H}. ESI-MS from acetronitrile solution (Figure S1b, Supplementary Information) : m/z^+: 368.76, 369.76 and 370.76 9 (obs.); m/z^+: 368.288, 369.288 (calcd. for Mn(Salophen)-H, and Mn(Salophen), respectively); $(m/z^+) + 1$: 370.766 (obs.); m/z^+: 782.679 (obs.), 782.611 (calcd for Mn(Salophen)-CN-Mn(Salophen)OH_2). IR (cm^{-1}; KBr, Figure S2, Supplementary Information): $\nu_{O\text{-}H}$, 3500–3376, 1607; $\nu_{C\text{-}H}$, 2922.4; $\nu_{C=N}$, 1579, ν ClO_4, 1146–1088 (multiplet), $\nu_{MnIII\text{-}O}$, 542.9; UV-Vis for Mn^{III}(Salophen) $(OH_2)_2{}^+$ (in aqueous medium, pH 5.62 ± 0.05) λ_{max}/nm (ε /dm^3 mol^{-1} cm^{-1}): 245 (38663 ± 942), 300sh (20320 ± 567), 340 (26593 ± 563), 425sh (9601 ± 265).

The GR grade (E. Merck) oxalic acid (H_2OX), perchloric acid and sodium hydroxide were used as received. Manganese(III) acetate dihydrate (Sigma Aldrich) and all other reagents were of highest grade purity available. Freshly prepared doubly distilled water as received from a borosilicate glass distillation setup was used for solution preparation; the second distillation was made through alkaline $KMnO_4$. Ionic strength was adjusted with $NaClO_4$. The stock solution of $NaClO_4$ was prepared and standardized as described earlier.[1] The stock solution of the complex (5×10^{-3} mol dm^{-3}, pH 5, 10% v/v MeOH/water) was protected from light and stored in a refrigerator at ~20 °C when not in use. It was not allowed to age for more than 24 h.

2.2 *Physical measurements*

A Perkin Elmer Lambda 25 UV-visible spectrophotometer with a matched pair of 10 mm quartz cells were used for all absorbance measurements. The IR measurements were made on a Perkin Elmer FTIR spectrometer Spectrum 2 using KBr pellet. ESR measurement was done on a JEOL (Japan) JES-FA 200 ESR spectrometer at room temperature operating in X-band mode (8.75–9.65 GHz, power 1.08 W, sensitivity 7×10^9 spins/0.1 mT, resolution 2.35 μT). The mass spectrum was recorded on a Macromass Q-TOF ESI-MS mass spectrometer. ^{1}H and ^{13}C NMR were performed

on a Bruker Avance-III 400 MHz NMR Spectrometer in DMSO-D_6. The DMSO signal (due to DMSO-H_6 present in the solvent) was split (3.720 and 2.492 ppm) indicating the fast exchange of the coordinated H_2O by DMSO ($Mn^{III}(OH_2)_2^+ + 2DMSO \rightleftharpoons Mn^{III}(DMSO)_2^+ + 2H_2O$, fast). A very broad signal at 26.521 ppm may be ascribed to that of the water protons while the ^1H signals of the aromatic salophen moiety are displayed at −17.359, −21.940 and −27.485 ppm (Figure S3a, Supplementary Information) as observed for this complex in CD_3OD by Ciringh *et al.*[8] The weak and broad imine proton resonance reported by Ciringh *et al.,* (at −398 ppm)[8] lies far beyond the accessible range probed in the present work. The chemical shifts of Mn^{III} Schiff base complexes have been attributed to the contact term which occurs through phenoxide oxygen and the imine group.[9] The signals (Figure S3b, Supplementary Information) for the aromatic carbons are observed at 209.678, 201.103 and 197.986 ppm and the one at 164.858 ppm is attributed to the imine carbons. The DMSO (^{13}C) signal is also split: 41.731 and 91.978 ppm, the former intense peak is assigned to the free DMSO while the later (weak) due to the DMSO coordinated to Mn^{III} centre signifies the fast exchange of DMSO with the H_2O coordinated to the metal centre. Fluorescence measurements were made on a JASCO fluorimeter model FP-8200 using Xe/D_2 light sources; bandwidth was set at 5 nm and scan speed was 100 nm/min. Cyclic voltammetry was performed using a Bioanalytical System Inc., USA epsilon electrochemical analyzer in conventional three-electrode configuration with bright platinum acting as the working electrode and Ag/AgCl, Cl^- (3.5 mol dm^{-3} KCl) as the reference electrode ($E^0_{AgCl/Ag}$ = 0.205 V at 25 °C).[10] The voltammograms (Figure S4 a,b, Supplementary Information) were recorded under a nitrogen atmosphere for an aqueous solution of the diaqua complex with tetrabutylammonium perchlorate serving as the supporting electrolyte. The pH measurements were made with Systronics (India) pH meter model 335 using a glass-Ag/AgCl, Cl^- (3 mol dm^{-3} NaCl) electrode CL 51. NBS buffers of pH 4.01, 6.86 and 9.20 prepared using KHphthalate, Na_2HPO_4/KH_2PO_4, and $Na_2B_4O_7{\cdot}10H_2O$, respectively, were used to calibrate the pH meter.[11] The measured pH values of the reaction medium were converted to p[H^+] (= −log[H^+] by a calibration curve using dilute $HClO_4$ solutions ($2.0 \times 10^{-2} \leq [H^+]/\text{mol dm}^{-3} \leq 1.0 \times 10^{-5}$) adjusted to I = 0.3 mol dm^{-3} ($NaClO_4$).[12]

2.3 *Kinetics*

The rate measurements were made under pseudo-first order conditions at $25.0 \leq T/°C \leq 40.0$. The reaction mixture in a 25.0 cm^3 measuring flask containing all components except the complex and the complex solution of known concentration (ionic strength adjusted to 0.3 mol dm^{-3}) were equilibrated separately in a water thermostat maintained at the desired temperature. After thermal equilibrium, a known volume of the complex solution (0.5 cm^3) was transferred in to the reaction mixture and volume was made up to the mark with distilled water at the same temperature and the desired solution was quickly transferred in to one of the optical cells housed in the thermostatted cell compartment of the spectrophotometer after rinsing. The other cell contained water as a reference. The absorbance change as a function of time was recorded at the preset wavelength (340 or 370 nm) at which the complex was the dominant absorbing species. The concentration of the complex was varied as $(3.0–5.0) \times 10^{-5}$ mol dm^{-3}. The methanol percentage in the actual reaction medium due to the addition of the complex solution (prepared in aqueous-methanol medium) was always kept constant (0.2% MeOH v/v). The pH of the reaction mixture was varied by self-buffering due to oxalic acid in the presence of dilute $HClO_4$ or NaOH. All rate measurements were made at constant ionic strength (I = 0.3 mol dm^{-3}) adjusted by $NaClO_4$.

The observed rate constants (k_{obs}) were calculated by fitting absorbance (A_t) –time (t) data to equation (1) by a nonlinear least squares computer program; ($A_0 - A_\infty$), k_{obs} and A_∞ were used as adjustable parameters.

$$A_t = (A_0 - A_\infty)\exp(-k_{obs}t) + A_\infty \quad (1)$$

The initial absorbance (A_0) was in the range of 0.6–0.9 and A_∞ was ≤ 0.25 and close to the fitted value; $\sigma(k_{obs})/k_{obs}$ was ≤ ± 5%. The very slow reactions ($k_{obs} \leq 4 \times 10^{-5}$ s^{-1}) were followed by initial rate method.[1] The rate data at 25 °C are collected in Table 1. The rate data at (30–40) °C and some representative kinetic plots are presented in the supporting information in the Table S1(a,b) and Figure S5(a–c), Supplementary Information, respectively, in Supplementary Information.

2.4 *Product analysis and stoichiometry*

The reaction mixture ($[Mn^{III}(salophen)(OH_2)_2^+] = 4 \times 10^{-3}$, $[H_2OX]_T$ = 0.04 mol dm^{-3}, ~10% MeOH/water) was set aside at 35 °C for calc. 10 $t_{1/2}$ and treated with a slight excess of $CaCl_2$ solution followed by aqueous NH_3. The white precipitate obtained was allowed to coagulate, collected by filtration, air dried and treated with dilute HCl. A colorless gas with effervescence (characteristic of CO_2) evolved. Our attempt for quantitative estimation of unreacted oxalate by $KMnO_4$ titration in the acid medium after quantitatively precipitating CaC_2O_4 from an aqueous NH_3 solution of the spent reaction mixture proved unsuccessful due to the presence of salophen ligand and the product manganese species.

Figure 1(a) and 1(b) depict the six-line ESR spectrum of the reaction mixture characteristic of Mn^{II}[1,2,13] establishing that the reaction we followed under different conditions of pH is in fact reduction of Mn^{III} in salophen scaffold by oxalate species. This is in line with what we reported earlier for the corresponding Mn^{III}(Salen) complex.[2] Based on these observations we assign the stoichiometry of the overall reaction as follows:

$$2Mn^{III}(Salophen)(OH_2)_2^+ + C_2O_4H^- + 3H^+ = 2Mn^{II} + 2H_2Salophen + 2CO_2 + 4H_2O \quad (2)$$

Table 1. Rate data for the reduction of Mn^{III}(salophen)$(OH_2)_2^+$ by oxalate species at 25.0 ± 0.1 °C.[a]

$[OX]_T$/mol dm^{-3}	pH	10^3k_{obs}/s^{-1}	10^3k_{cal}/s^{-1}	$[OX]_T$/mol dm^{-3}	pH	10^3k_{obs}/s^{-1}	10^3k_{cal}/s^{-1}
0.007	1.79	0.03	0.032	0.05	1.11	0.83	1.14
0.01	1.73	0.06	0.063	0.05	0.91	0.72	1.12
0.01	1.56	0.054	0.065	0.05	0.77	0.76	1.06
0.01	1.43	0.06	0.067	0.05	0.67	0.67	0.99
0.01	1.25	0.049	0.067	0.06	1.30	1.31	1.47
0.01	0.98	0.038	0.063	0.07	1.26	2.00	1.88
0.01	0.80	0.05	0.056	0.08	1.22	2.49	2.32
0.01	0.69	0.04	0.051	0.09	1.19	2.88	2.78
0.01	0.59	0.03	0.046	0.10	1.16	3.36	3.26
0.02	1.59	0.20	0.225	0.10	1.26	2.96	3.16
0.02	1.67	0.17	0.221	0.10	1.32	2.94	3.08
0.02	1.84	0.17	0.212	0.10	1.39	2.97	3.00
0.02	1.89	0.16	0.209	0.10	1.47	2.96	2.89
0.02	1.92	0.15	0.208	0.10	1.55	2.92	2.79
0.02	1.96	0.15	0.206	0.10	1.80	2.52	2.50
0.02	2.04	0.16	0.203	0.10	1.98	2.28	2.33
0.02	2.07	0.16	0.202	0.05	1.95	1.28	0.894
0.02	2.35	0.15	0.197	0.10	1.93	3.17	2.37
0.02	2.75	0.14	0.20	0.15	1.85	4.59	4.13
0.03	1.49	0.42	0.461	0.20	1.83	5.58	5.92
0.04	1.38	0.69	0.761	0.25	1.82	7.49	7.75
0.05	1.35	0.96	1.09	0.10	2.29	2.20	2.15
0.05	1.28	0.75	1.11	0.01	3.66	0.030	0.063
0.05	3.77	0.35	0.601	0.02	3.34	0.08	0.201
0.06	3.79	0.44	0.742	0.02	3.75	0.050	0.177
0.07	3.85	0.81	0.85	0.03	3.73	0.16	0.316
0.08	3.82	1.06	1.03	0.04	3.74	0.25	0.46
0.08	3.80	0.79	1.04	0.08	3.62	1.18	1.16
0.08	3.28	1.54	1.36	0.08	3.38	1.43	1.31
0.01	4.24	0.02	0.048	0.02	4.26	0.07	0.133
0.03	4.23	0.13	0.23	0.04	4.29	0.21	0.327
0.05	4.21	0.36	0.45	0.06	4.25	0.52	0.54
0.07	4.22	0.81	0.67	0.08	4.05	1.43	0.87
0.08	4.26	1.06	0.76	0.08	4.41	0.55	0.69
0.08	4.47	0.52	0.67	-	-	-	-

[a] λ /nm = 340, $[complex]_T = (4-5) \times 10^{-5}$ mol dm^{-3}, I = 0.3 mol dm^{-3}; pH = $-\log[H^+]$. pK_1 = 1.01, pK_2 = 3.60 for H_2OX: Martell A E and Smith R M 1977 *Critical Stability Constants* (New York: Plenum Press) vol. 3, p.92.

2.5 *Test of free radical*

A few runs were made in the presence of acrylamide monomer. The purpose was to test the presence of radical through polymerization of acrylamide monomer and examine its influence on the reaction rate. The reaction carried out at 40 °C (I = 0.3, $[complex]_T = 4.0 \times 10^{-5}$, $[OX]_T$ = 0.03 mol dm^{-3}, λ /nm = 340) in the presence of [acrylamide] = 0, 0.01, 0.02, 0.03 mol dm^{-3} (pH = 1.47 ± 0.01) yielded 10^3k_{obs}/s^{-1} as 1.15 ± 0.03, 1.14 ± 0.03, 1.04 ± 0.02, 1.17 ± 0.06, respectively, indicating thereby negligible influence of the monomer. Further, we did not observe any polymerization of acrylamide. A similar observation was made by us in our previous study on oxalate oxidation by Mn^{III}(Salen).[2] The formation of the oxalate radical($C_2O_4^{-\cdot}$) and its decomposition product, $CO_2^{-\cdot}$ have been reported earlier.[14,15] In order to account for the 2:1 stoichiometry, we conclude that the radical $C_2O_4^{-\cdot}$. (≡ $CO_2^{-\cdot} + CO_2$) must undergo fast oxidation by available Mn^{III}(Salophen)$^+$ prior to being scavenged by acrylamide, the congener of its polymer.

2.6 *DFT calculations*

The TURBOMOLE 6.4 package was adopted to perform all calculations using density functional theory (DFT).[16,17] The structure optimization was accomplished by the BP86 functional and def2-TZVPP basis set along with the resolution –of-identity (RI) approximation[18–20] (RI-BP86/def2-TZVPP in brief). Further details of the energy, graphical presentations and computation of the bond parameters of the complexes are mentioned in our earlier work.[2]

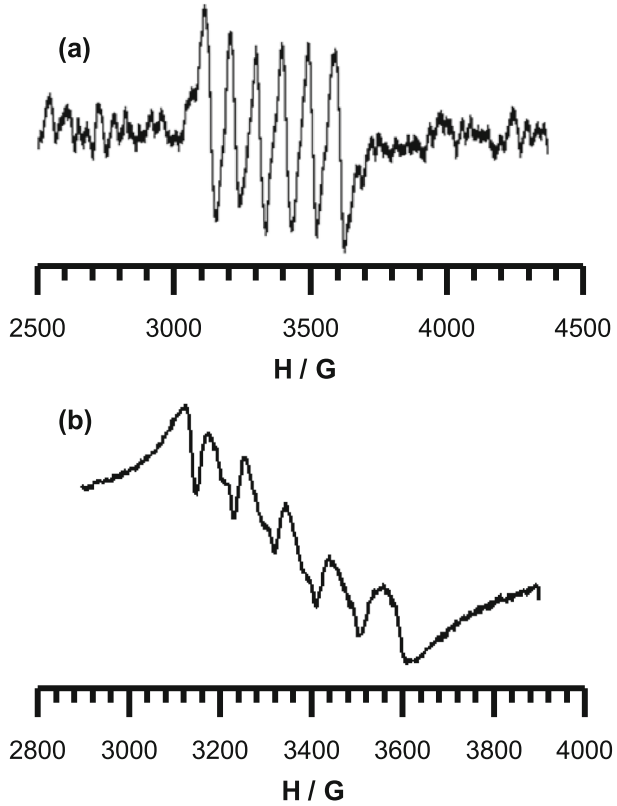

Figure 1. (a) Six-line ESR spectrum (X-band, room temperature) of the product Manganese(II) in solution after completion of the reaction of $Mn^{III}(Salophen)(OH_2)_2^+$ with H_2OX at pH ~1.5, 30 °C. Intensity vs H (Gauss) plot, g = 2.0, hyperfine const. A = 96 G. (b) Six-line ESR spectrum (X-band) of the product Mn(II) species at 100 K; Mn^{III}(Salophen) was allowed to react with oxalate species at pH = 3.6 (40 °C). Intensity vs H (Gauss) plot, g = 2.0, hyperfine const. A = 85 G.

3. Results and Discussion

3.1 *Preliminary observations*

The time-dependent spectral scans at pH 1.46 (35 °C) for the reaction mixture display an isosbestic point around 465 nm (Figure S6a in Supplementary Information). The maximum around 340 nm and the shoulders at 300 and 425 nm characteristic of the parent complex tends to disappear with time due to its reduction by oxalate species. A similar observation was also made when the reaction was conducted at pH 2 (Figure S6 b,c, Supplementary Information).

3.2 *Cyclic voltammetry*

The CV scan for the diaqua complex shows discernible peaks at −134 mV (cathodic) and +402 mV (anodic). The system is, however, a quasi-reversible one as evidenced from the loss of reversibility in the repeat scans (Figure S4 a,b in Supplementary Information).

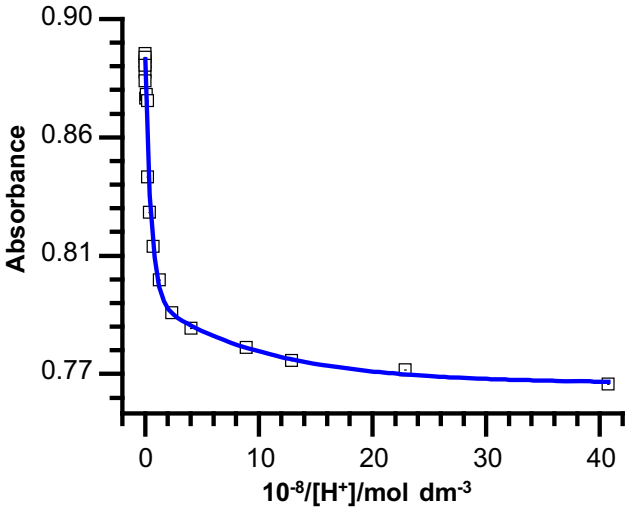

Figure 2. Absorbance (A) vs. $(10^{-8}/[H^+])/dm^3\,mol^{-1}$ plot, λ = 340 nm; $[Mn^{III}(Salophen)(OH_2)_2^+]_{total} = 4.0 \times 10^{-5}$ mol dm^{-3}, I = 0.3 mol dm^{-3}, 30.0 °C.

3.3 *pK_M of Mn^{III} (Salophen)$(OH_2)_2^+$*

The pK_M of the diaqua complex was determined at 30 °C by measuring its absorbance (340 nm) of a constant concentration (= 4.0×10^{-5}, I = 0.3 mol dm^{-3}) as a function of pH (5.65 ≤ pH ≤ 9.61, morpholine/$HClO_4$ buffer). The nature of the plot of absorbance (A) vs. $10^{-8}/[H^+]$ (Figure 2) is consistent with the acidic dissociation of only one coordinated water molecule (Eq. 3).

$$Mn^{III}(salophen)(OH_2)_2^+ \underset{}{\overset{K_M}{\rightleftharpoons}} Mn^{III}(salophen)(OH)(OH_2) + H^+ \qquad (3)$$

Accordingly, the absorbance (A) – pH data were analyzed by Eq. (4)

$$A = (A_0 + A'\,K_M/[H^+])/(1 + K_M/[H^+]) \qquad (4)$$

where, A_0, A and A' denote the absorbance of the complex when it exists only in the diaqua form, as an equilibrium mixture of the di-aqua and aqua-hydroxo species at the experimental pH and as aqua–hydroxo species, respectively. A_0, (A' K_M) and K_M were varied and A-pH data were fitted to equation (4) by a nonlinear least squares program. We obtained K_M/mol dm^{-3} = $(1.6 \pm 0.2) \times 10^{-8}$ (pK_M = 7.80 ± 0.05), A_0 = 0.889 ± 0.003, A' K_M/mol dm^{-3} = (1.21 ± 0.16) × 10^{-8}.

The value of pK_M was further checked by fluorescence intensity (F) measurements of the diaqua

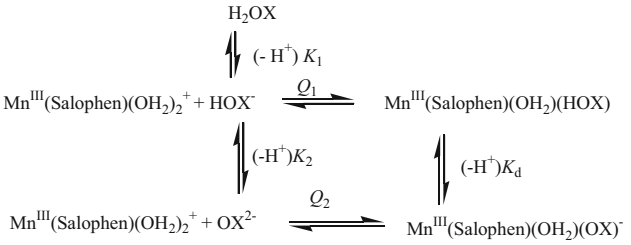

Scheme 1. Fast equilibria preceding the redox reaction.

complex (1.0×10^{-5} mol dm^{-3}) at 450 nm (λ_{exc} = 340 nm) which was enhanced significantly as pH was raised from 3 to 9 (Figure S7, Supplementary Information). Only one inflexion point in the F_{obs} vs. pH curve was observed consistent with the formation of the monohydroxo species which displayed fluorescence (F_2) higher than its diaqua analogue (F_1). The fluorescence data were fitted to Eq. (5) (equivalent to Eq. (4) using $1/[H^+] = \exp(2.303pH)$) and we obtained $F_1 = 348.25 \pm 16.02$, $F_2K_M = (5.2 \pm 1.9) \times 10^{-4}$, $K_M = (7.13 \pm 2.73) \times 10^{-7}$ mol dm^{-3} ($pK_M = 6.15 \pm 0.17$ at 26.0 °C, $I = 0.3$ mol dm^{-3}).

$$F_{obs} = \frac{F_1 + F_2K_M \exp(2.303pH)}{1 + K_M \exp(2.303pH)} \quad (5)$$

3.4 *Equilibrium constants Q_1, and K_d*

The ^{1}H NMR measurement in DMSO-D$_6$ (see Experimental Section) indicates that the replacement of the Mn^{III} bound aqua ligand by oxalate species is a rapid and equilibrium controlled process. We attempted to study the equilibria (Scheme 1) spectrophotometrically (370 nm) at 30 °C; the concentration of the diaqua complex was fixed at 4.0×10^{-5} and $[OX]_T$ was varied at constant pH ($[OX]_T$ = 0.005–0.1, and 0.002–0.08 mol dm^{-3} at pH = 2.23 ± 0.2 and 3.72 ± 0.02, respectively). Under these pH conditions the oxalate species are OX^{2-} and HOX^- (pK_1 = 1.0, pK_2 = 3.58 for H_2OX, 30 °C, I = 0.3 mol dm^{-3})[2] and the redox reaction is too slow to interfere with the equilibria depicted in Scheme 1. Relevant data are shown in Figure S8(a,b) in Supplementary Information.

The extrapolated zero time absorbance (A) of the reaction mixtures (relative to the corresponding solution in absence of the complex) is given by Eq. (6):

$$A = \frac{A_0 + [(A_1 + A_2\, k_d/[H^+])\, Q_1 f_2][OX]_T}{1 + [(1 + k_d/[H^+])\, Q_1 f_2][OX]_T} \quad (6)$$

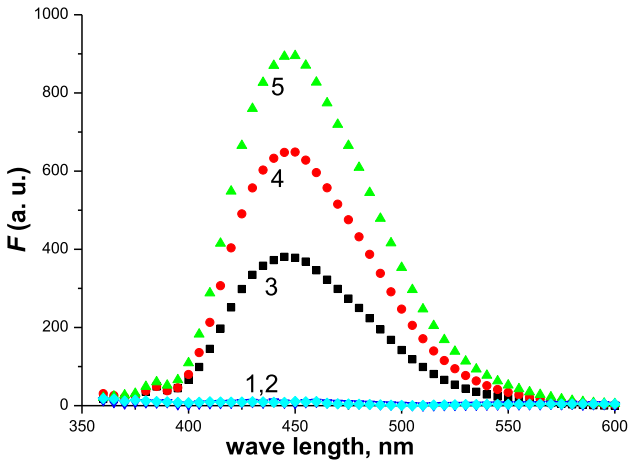

Figure 3. Fluorescene spectra of Mn^{III}(Salophen)(OH$_2$)$_2^+$ in the absence and presence of oxalate at 27 °C, pH = 3.81 ± 0.03, $\lambda_{exc.}$/nm = 340.0. $[complex]_T$, $[OX]_T$/mol dm^{-3} (curve no.): 0.00,0.001 (1); 0.00, 0.01 (2); 1.0×10^{-5}, 0 (3); 1.0×10^{-5}, 0.001 (4); 1.0×10^{-5}, 0.01 (5).

where, A_0, A_1 and A_2 denote absorbances of the di-aqua-, its bi-oxalato- and oxalato-complexes, respectively, for the same total concentration and $f_2 = K_1[H^+]/([H^+]^2 + K_1[H^+] + K_1K_2)$. The $A - [OX]_T$ data were fitted to Eq. (6) by a nonlinear least squares computer program. From the calculated values of $[(1 + K_d/[H^+])Q_1 f_2]$ we obtained $K_d = (1.8 \pm 0.2) \times 10^{-3}$ mol dm^{-3} and $Q_1 = 10.4 \pm 0.3$ dm^3 mol^{-1} (30 °C) (see captions of Figure S8 a,b, Supplementary Information).

Figure 3 displays the enhancement of the fluorescence intensity of the complex in the presence of oxalate. A check for the values of Q_1 and K_d was also performed by the fluorescence intensity measurements of the complex in the presence of oxalate under varying conditions of pH and $[OX]_T$ (2.05 ± 0.03 ≤ pH ≤ 5.06 ± 0.03, $1.0 \times 10^{-4} \le [OX]_T$/mol dm^{-3} ≤ 0.1) at a constant concentration of the diaqua complex, 1.0×10^{-5} mol dm^{-3}. The observed fluorescence intensity of the reaction mixture (F_{obs}) showed a decreasing trend with time at a relatively high concentration of oxalate indicating minor interference presumably due to the reduction of Mn^{III} centre (see later). Hence all F_{obs} data were corrected for this change by extrapolation to zero time (i.e. after 40 s of mixing) which invariably was of the form $F_{obs} = a - bt$ for a small time span. The relevant data are collected in Table S2, Supplementary Information and further details of data analysis are presented in Appendix A. The calculated values of Q_1 (= 13.5±8.2 dm^3 mol^{-1}) and $10^3 K_d$ (= 3.8±2.5 mol dm^{-3}, 26 °C) agree well with those obtained by the absorbance measurements.

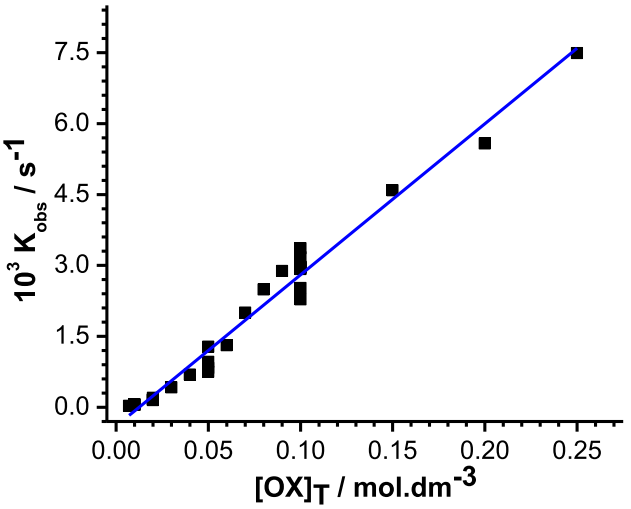

Figure 4. $10^3 k_{obs}/s^{-1}$ vs. $[OX]_T/mol\,dm^3$ plot at 25 °C ($1.1 \leq pH \leq 2.07$): $10^3 k_{obs} = P_1[OX]_T^2/(1 + P_2[OX]_T)$, $P_1 = (1.65 \pm 0.43) \times 10^3$, $P_2 = 49.8 \pm 15.3$.

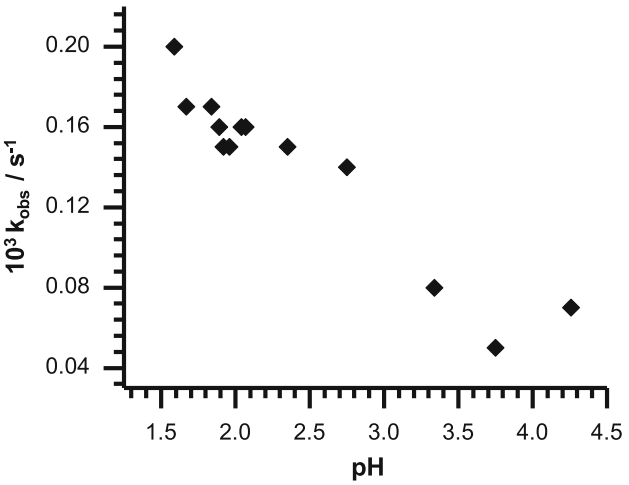

Figure 5. $10^3 k_{obs}/s^{-1}$ vs. pH plot at 25 °C, $[OX]_T/mol\,dm^{-3} = 0.02$.

3.5 *Analysis of the kinetic data*

A preliminary study indicated that the diaqua complex is substantially stable to acid catalyzed thermal decomposition (see Figure S9 in Supplementary Information). A typical plot of $10^3 k_{obs}$ vs. $[OX]_T$ (= 0.007–0.25 mol dm^{-3}; $1.1 \leq pH \leq 2.07$) at 25 °C shows a nonlinear variation of k_{obs} with greater than first order dependence on $[OX]_T$ (Figure 4).

A similar trend is evident also at higher pH and at all other temperatures. The pH dependence of k_{obs},however, indicates that OX^{2-} contrastingly is a much weaker reducing species than HOX^- (Figure 5) in the present context further supporting our earlier observation on the Mn^{III}(Salen) + oxalate.[2]

Scheme 2, in addition to Scheme 1, is proposed to interpret the rate data (see Table 1 and Table S1a,b in Supplementary Information). Accordingly, k_{obs} takes the form:

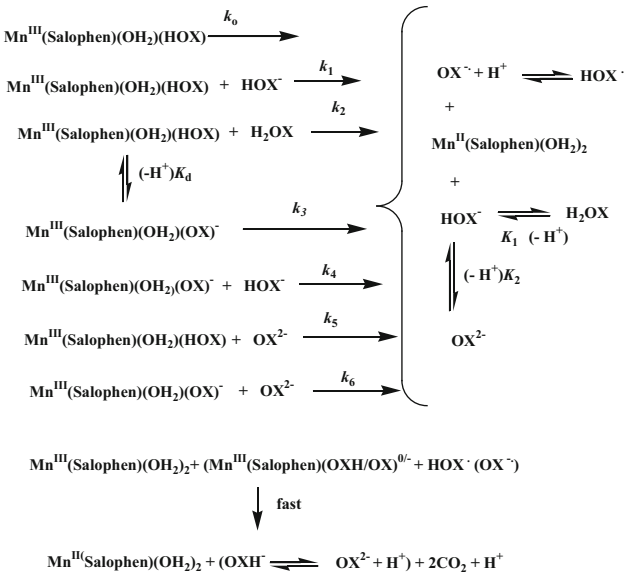

Scheme 2. Reduction of Mn^{III}(Salophen) by oxalate speci[es].

$$k_{obs} = \frac{k_0 Q_1 f_2[OX]_T + k_1 Q_1 (f_2[OX]_T)^2 + k_2 Q_1 f_1 f_2 [OX]_T^2 + k_3 K_d Q_1 f_2 [OX]_T/[H^+] + k'(f_2[OX]_T)^2/[H^+] + k_6 k_d K_2 Q_1 (f_2[OX]_T/[H^+])^2}{1 + K_M/[H^+] + Q_1 f_2 [OX]_T (1 + K_d/[H]^+)} \quad (7)$$

where, $k' = (k_4 K_d + k_5 K_2) Q_1$, $f_1 (= [H^+]^2/([H^+]^2 + K_1[H^+] + K_1 K_2))$ and $f_2 (= K_1[H]/([H^+]^2 + K_1[H^+] + K_1 K_2))$ denote the fractions of $[OX]_T$ as H_2OX and HOX^-, respectively. The parameters $(k_0 Q_1)$, $(k_1 Q_1)$, $(k_2 Q_1)$, $(k_3 K_d Q_1)$, k', $(k_6 K_d K_2 Q_1)$, Q_1 and K_d were varied to fit the rate data to Eq. (7) by a nonlinear least squares program. The initial inputs of the parameters (Q_1, K_d) were chosen from the equilibrium measurements and the analysis of the rate data using the limiting forms of Eq. (7) at $0.5 \leq pH \leq 2.0$ and $3.0 \leq pH \leq 4.5$. The acid dissociation equilibrium of the diaqua complex was neglected ($K_M/[H^+] <<< 1$). The reduction of Mn^{III}(salophen) $(OH_2)_2^+$ by H_2OX ($Mn^{III}(Salen)(OH_2)_2^+ + H_2OX \rightarrow$ Products; k_{H2OX}) when included in the proposed Scheme 2, did not improve data fitting and gave the statistically

Table 2. Calculated values of the rate and equilibrium parameters.[a,b]

Temp.→	25.0 ± 0.1 °C	30.0 ± 0.1 °C	35.0 ± 0.1 °C	40.0 ± 0.1 °C
k_oQ_1	0.00	0.00	0.00	0.00
k_1Q_1	0.636 ± 0.031	0.654 ± 0.073	0.780 ± 0.078	0.85 ± 0.21
k_2Q_1	2.20 ± 0.12	2.70 ± 0.23	3.85 ± 0.21	7.00 ± 0.36
$k_3K_dQ_1$	0.00	0.00	0.00	0.00
$k'Q_1$	$(6.76 \pm 1.05) \times 10^{-4}$	$(7.0 \pm 6.0) \times 10^{-4}$	$(10.0 \pm 5.1) \times 10^{-4}$	$(17.0 \pm 4.7) \times 10^{-4}$
$k_6K_dK_2Q_1$	$(3.98 \pm 1.19) \times 10^{-8}$	$(4.9 \pm 5.4) \times 10^{-8}$	$(6.0 \pm 4.7) \times 10^{-8}$	$(7.00 \pm 4.27) \times 10^{-8}$
Q_1	22	15	16	16
K_M	7.1×10^{-7}	7.1×10^{-7}	7.1×10^{-7}	7.1×10^{-7}
K_d	1.0×10^{-3}	1.5×10^{-3}	1.2×10^{-3}	1.0×10^{-3}
k_0	0.00	0.00	0.00	0.00
k_1	$(2.89 \pm 0.14) \times 10^{-2}$	$(4.36 \pm 0.49) \times 10^{-2}$	$(4.87 \pm 0.49) \times 10^{-2}$	$(5.31 \pm 1.31) \times 10^{-2}$
k_2	$(10.0 \pm 0.54) \times 10^{-2}$	$(18.0 \pm 1.53) \times 10^{-2}$	$(24.1 \pm 1.3) \times 10^{-2}$	$(43.75 \pm 2.25) \times 10^{-2}$
k_3	0.00	0.00	0.00	0.00
k_4[c]	$(1.53 \pm 0.24) \times 10^{-2}$	$(1.55 \pm 1.33) \times 10^{-2}$	$(2.60 \pm 1.32) \times 10^{-2}$	$(5.31 \pm 1.47) \times 10^{-2}$
k_5[c]	$(6.11 \pm 0.95) \times 10^{-2}$	$(8.88 \pm 7.60) \times 10^{-2}$	$(11.1 \pm 5.6) \times 10^{-2}$	$(18.0 \pm 5.0) \times 10^{-2}$
k_6	$(0.72 \pm 0.21) \times 10^{-2}$	$(0.83 \pm 0.93) \times 10^{-2}$	$(1.11 \pm 0.87) \times 10^{-2}$	$(1.48 \pm 0.91) \times 10^{-2}$
χ^{2d}	2.85	18.04	9.16	21.12

[a]Rate constants (k_is, i = 0–6) are not corrected for stoichiometry. Calcd. values of k_oQ_1 and k_3KdQ_1 are $(0.003 \pm 1.7) \times 10^{-3}$, $(0.00035 \pm 3.9) \times 10^{-6}$ (25 °C); $(1.8 \pm 3.5) \times 10^{-3}$, $(0.0011 \pm 1.32) \times 10^{-7}$ (30 °C), respectively. [b]units : s^{-1} (k_0, k_3); $dm^3\ mol^{-1}\ s^{-1}$ (k_1, k_2, k_4, k_5, k_6); $dm^3\ mol^{-1}$ (Q_1), and mol dm^{-3} (K_d, K_M, K_2). [c]$k_4 = k'/(2K_d)$; $k_5 = k'/(2K_2)$. [d]$[10^3(k_{cal}–k_{obs})]^2$.

insignificant value of the corresponding rate constant. Hence, it was omitted. Also, the parameters (k_oQ_1) and ($k_3K_dQ_1$) turned out statistically insignificant (see footnote *a* of Table 2). Hence these two parameters were set to zero in the final calculation. Figure 6 and a comparison of k_{cal} with k_{obs} in Table 1 are supportive of the proposed Scheme 2 (see Table S1a,b and Figure S10a–c, Supplementary Information, for 30–40 °C). The calculated values of the parameters are collected in Table 2. The rate constants k_4 and k_5 were calculated from the values of k' considering the cyclic Scheme 3 for which $k_4K_d = k_5K_2$ is valid through $K_{eq} = K_d/K_2$ and $k_5 = k_4K_{eq}$.

The activation parameters for the rate determining paths are presented in Table 3.

3.6 *Computed structures (DFT)*

Figure 7 delineates the structures of the diaqua- and different oxalate- complexes of Mn^{III}(Salophen) with selected bond parameters listed in Table S3 (Supplementary Information). The X-ray crystallography of $[Mn^{III}(Salophen)(OH_2)(CH_3OH)](ClO_4)$[21] and $[Mn^{III}(Salophen)(C_2H_5OH)_2](BPh_4)$[22] have been reported. The bond distances (Å), Mn-O(phenoxide) (1.859, 1.875[21]; 1.85,1.85[22]) and Mn-N(imine) (1.981, 1.987[21]; 1.97,1.99[22]) for these two complexes are in good agreement with those for the diaqua and other (aqua)(oxalate) complexes (Table S3, Supplementary Information) while the *trans*-di-axial bonds

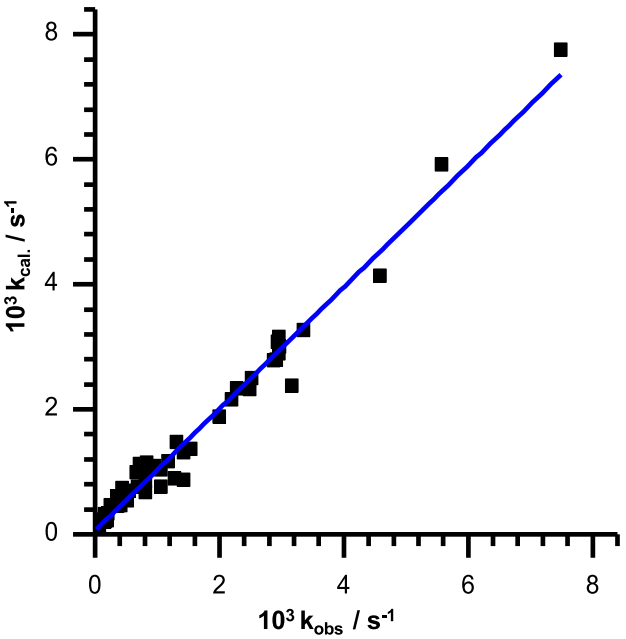

Figure 6. Correlation plot ($10^3k_{cal}/s^{-1}$ vs. $10^3k_{obs}/s^{-1}$) at 25 °C.

for the diaqua complex is significantly longer (0.126- 0.145 Å[21]; 0.137–0.147 Å[22]) than the corresponding (aqua)(methanol) and bis(ethanol) complexes. All such complexes show the distorted octahedral arrangement of the ligands with Mn^{III} marginally above the pseudo-square plane. While no hydrogen

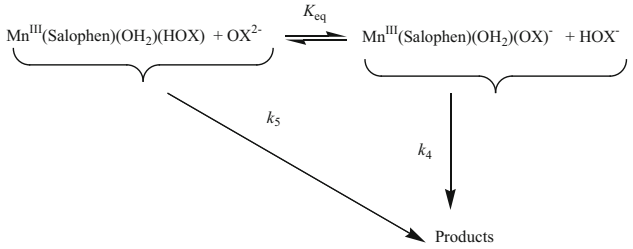

Scheme 3. Evaluation of k_4 and k_5.

bonds between the coordinated phenoxide and apical H_2O (and CH_3OH) were detected, intermolecular H-bonding interaction was observed in the crystal of the bis(ethanol) complex cation.[22] No intramolecular H-bonding was detected by us for the diaqua complex. However, H-bonding with varying degree of stability as indicated by H-bond distances could be observed in different oxalate species of Mn^{III}(Salophen) (B, C, D, E, F). The oxalate complexes may be scaled in terms of their ground state complexation energy (E) as E < F < G < B < C < D to which both overall charge and hydrogen bonding presumably contributes.

3.7 *Mechanism of redox reaction*

The reduction of Mn^{III}(Salophen) by oxalate species is preceded by much faster equilibrium formation of its mono-oxalato complexes with HOX^- and OX^{2-}. The values of the formation equilibrium constant for [Mn^{III}(Salophen)(OH_2)HOX] obtained from equilibrium and kinetic measurements are comparable but somewhat lower than the corresponding Mn^{III}(Salen) species ($Q_1 = 42\,dm^3\,mol^{-1}$ 25–40 °C).[2] Also, it is to be noted that the [Mn^{III}(Salophen)(OH_2)HOX] is a stronger acid than its *Salen* counterpart (pK = 2.74 vs 3.33[2] at 30 °C, $I = 0.3\,mol\,dm^{-3}$). These differences might be related to the accessible H-bonded conformers (Figure 5, structures $D_1 - D_4$ for Mn^{III}(Salen)(OH_2)(HOX))[2] due to the flexibility of the ethylene bridge which is not possible for its Salophen analogue due to the intervening rigid aromatic ring. In contrast, the electronic effect of the conjugated aromatic rings for the latter complex is favourable to enhance the acidity of the mono bonded HOX^- as observed.

The intramolecular reduction of Mn^{III} by the coordinated oxalate species for Mn^{III}(Salophen)(OH_2)(HOX/OX)$^{0/-}$ is not observed. Such reaction is also statistically insignificant for the corresponding *Salen* complex[2] further demonstrating the effect of complex formation on the redox stability of the Mn^{III} centre. H_2OX alone is not a reducing species. The observed reactivity trend: $k_2 > k_1 \geq k_4 < k_5 > k_6$ ($k_0, k_3 \sim 0$) is worth noting. The kinetically most important reaction is the reduction of Mn^{III} in Mn^{III}(Salophen)(OH_2)(HOX) by H_2OX (k_2/k_1 = 3–8 at 25–40 °C, Table 2). The precursors of the k_1 and k_2 paths (structures E and F, Figure 7) could not be identified by the equilibrium measurements due to their low thermodynamic stabilities. However, their subtle kinetic consequence in Mn^{III} reduction is notable. A rate comparison for the k_1 vs k_2 paths for *Salen* and *Salophen* complexes in Table 4 clearly shows that the former complex is more sensitive to reduction than the latter despite the fact that the central aromatic ring, due to its relatively stronger electron withdrawing effect, is likely to favour facile electron transfer to Mn^{III} centre through the bound HOX species than the aliphatic ethylene bridge.

The basicity difference for the coordinated phenoxides in these complexes, Mn^{III}(Salophen) <Mn^{III}(Salen), appears to be a significant factor in controlling the dynamics of electron transfer through H-bonding (see Figure 7 of ref 2). In other words, all these observations distinctly speak of the effect of hydrogen bonding and the involvement of *proton controlled electron transfer process* (PCET) as we proposed for the corresponding Salen complex.[2] The activation parameters for k_1, k_4, k_5, and k_6 paths are low and comparable with each other averaging to $\Delta H^{\neq}_{av.} = 41.6 \pm 5.3\,kJ\,mol^{-1}$ and $\Delta S^{\neq}_{av.} = -136 \pm 23\,J\,K^{-1}\,mol^{-1}$. This entails the fact that the overall energy demand in attaining the transition state of the electron transfer process is low and virtually similar in magnitude despite the difference in the reductant oxalate species. The corresponding large negative $\Delta S^{\neq}_{av.}$ value supposedly point to the considerable ordering in assembling the transition state. In contrast, the substantially high values of

Table 3. Activation parameters for the rate controlling paths.

Paths →	k_1	k_2	k_4	k_5	k_6
$\Delta H^{\neq}$/kJ mol^{-1}	36.2 ± 7.4	71.6 ± 6.0	57.7 ± 9.9	52.1 ± 3.1	33.7 ± 2.6
$\Delta S^{\neq}$/J K^{-1} mol^{-1}	−153 ± 25	−24 ± 19	−86 ± 33	−93 ± 10	−173 ± 9

[a] $k_i = (k_B T/h)\exp(-\Delta H^{\neq}/RT + \Delta S^{\neq}/R)$.

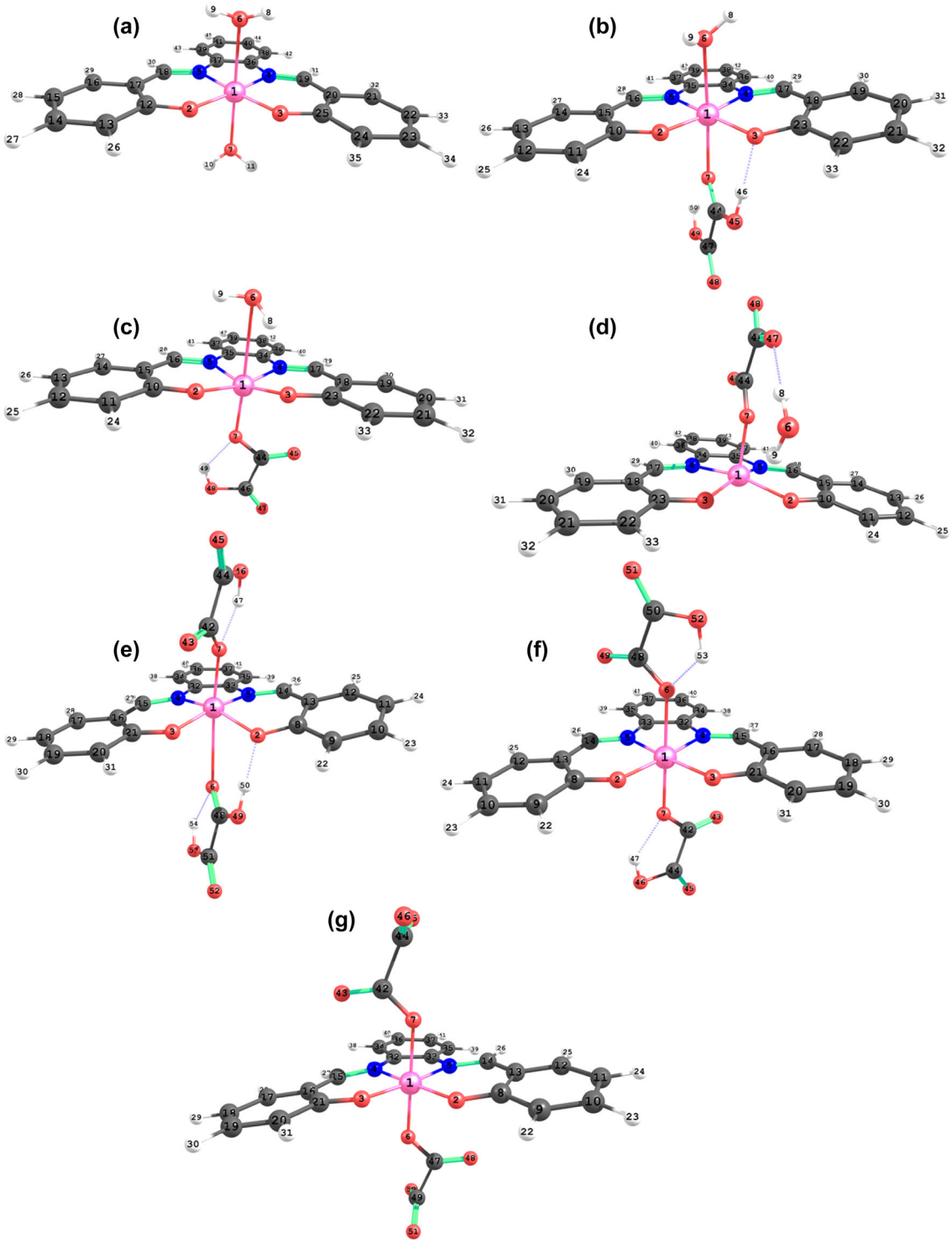

Figure 7. RI-BP86/def2-TZVPP optimized structures of *trans*-Mn^{III}(Salophen)$(OH_2)_2{}^+$(**A**), Mn^{III}(Salophen)$(OH_2)(H_2OX)^+$ (**B**), Mn^{III}(Salophen)(OH_2)(OXH) (**C**), Mn^{III}(Salophen)$(OH_2)(OX)^-$ (**D**), Mn^{III}(Salophen)(HOX)(H_2OX) (**E**), Mn^{III}(Salophen)$(HOX)_2{}^-$ (**F**), Mn^{III}(Salophen)$(OX)_2{}^{3-}$ (**G**). HOX^-/OX^{2-} : $^-$O-C(=O)CO_2H/$^-O_2$C-CO_2^-.

the activation parameters for the k_2 path (Table 3) is a reflection of the reorganizational disorder in attaining the transition state in this path. A similar observation was also made on the corresponding *Salen* complex.[2] The similarity in the mechanism of reduction via k_1 and k_2 paths is also indicated by the isokinetic relationship:

Table 4. Rate comparison for Mn^{III}(Salen)[a] and Mn^{III}(Salophen).

Temp.,°C	$k_1^{Salen}/k_1^{Salophen}$	$k_2^{Salen}/k_2^{Salophen}$
25.0	25.2 ± 4.3	73.9 ± 11.0
30.0	19.9 ± 2.7	57.8 ± 8.3
35.0	23.8 ± 2.8	81.3 ± 8.3
40.0	32.6 ± 9.2	61.0 ± 10.9

[a] See Table 2 of Ref. [2].

$T_{iso}/K = (\Delta H^{\pm}_2 - \Delta H^{\pm}_1)/(\Delta S^{\pm}_2 - \Delta S^{\pm}_1)$ (= 274 ± 29.7) where T_{iso} denote the isokinetic temperature and the subscripts refer to the paths.

3.8 *Relevance to Oxalate Oxidase*

Oxalate oxidase (OXO, EC 1.2.3.4)[23,24] is a Mn^{II} containing enzyme which catalyzes the oxidation of oxalate by oxygen. The crystallographic study[24] of this enzyme from barley has revealed its hexameric structure comprising a trimer of dimers with one active site Mn(II) per protein subunit; Mn(II) has *cis*-octahedral coordination environment with three histidines (ϵ-*N* coordination), one glutamate, and two H_2O molecules, the water molecules being in the *cis* disposition unlike in the $[Mn^{III}(Salophen/Salen)(OH_2)_2]^+$. Opaleye *et al.,*[24] proposed a catalytic mechanism for OXO which involves O_2 for H_2O substitution at the Mn^{II} centre to which HOX is vicinally coordinated. This is followed by intramolecular electron transfer from Mn^{II} to the coordinated O_2 forming superoxide (still coordinated to Mn^{III} centre) and transforming Mn^{II} to Mn^{III}. The Mn^{III}-HOX-$O_2^{\cdot}$ intermediate then undergoes redox transitions following several intramolecular paths finally resulting in the oxidized products, CO_2 and H_2O_2 (Figure 6 of ref. 24) and regenerating the enzyme. While the process of oxalate oxidation by OXO is a catalytic one, our system with distal coordination of HOX^- relative to the coordinated H_2O is stoichiometric in nature *in vitro*. But both involve Mn^{III} and Mn^{II} intermediates with mono dentate coordination of HOX^- to Mn centre and function under similar pH conditions (pH ∼ 4). The *trans*-Mn^{III}(Salen/Salophen) $(OH_2)_2^+$-oxalate system coupled with the superoxide activity (SOD) of these synthetic enzymes can also function as a catalytic system for oxalate oxidation as,

$$Mn^{II}(Salen/Salophen) + O_2^{-\cdot} + 2H^+ \rightarrow Mn^{III}(Salen/Salophen) + H_2O_2$$

is the possible path of the regeneration of the reactant Mn^{III} complex, while the toxic H_2O_2 can be taken care of by their catalase activity.[25–28] In addition, the generated H_2O_2 in the net enzymatic action of the Mn^{III}(Salen/Salophen) in the oxalate oxidation may find a useful application in plant biochemistry in terms of cell-wall cross-linking, and fungicidal activity.[23] It is further pertinent to note that humans and many other animals lacking in the enzyme OXO suffer from serious health hazards like a chronic renal disease, liver damage, etc., due to the improper and uncontrolled metabolism of oxalate.[30] In that context, Mn^{III}(Salen/Salophen) type of complexes may prove to be OXO mimetics considering their abilities to oxidize oxalate to CO_2 while acting as SOD and catalase mimics.[31]

4. Conclusions

The oxalate oxidation by $Mn^{III}(Salophen)(OH_2)_2^+$ proceeds with the prior equilibrium formation of Mn^{III}(Salophen)(OH_2)(HOX) which further undergoes acid dissociation to $[Mn^{III}(Salophen)(OH_2)(OX)]^-$ (pK = 2.7 at 25–40 °C, I = 0.3 mol dm^{-3} $NaClO_4$). These mono oxalato complexes do not show sign of intramolecular electron transfer from the oxalate moiety to Mn^{III} centre. The redox reactions of these two mono bonded complexes occur *via* second-order processes involving H_2OX, HOX^- and OX^{2-}; the kinetic data have been analyzed carefully and the rate and activation parameters of each of the paths have been reported. The kinetic data reflect that the reduction of Mn^{III} centre in Mn^{III}(Salophen)(OH_2)(HOX) by H_2OX is the fastest and of $[Mn^{III}(Salophen)(OH_2)(OX)]^-$ by OX^{2-} is the slowest. Molecular modeling and structure optimization by DFT showed the involvement of hydrogen bonds in the complexes which favour the assembling of the required transition state. A comparative analysis of the rate constants and activation parameters delineate the coupling of proton transfer with electron transfer invoking the proton controlled electron transfer (*PCET*) kinetics. The relevance of *trans*-$[Mn^{III}(Salophen/Salen)(OH_2)_2]^+$ to the enzyme Oxalate Oxidase (OXO) in oxalate oxidation is highlighted.

Supporting Information (SI)

Figures S1(a,b), S2(a,b), S3(a,b), S4(a,b), S5(a–c), S6(a–c), S7, S8(a,b), S9, S10, Tables S1(a,b), S2 and S3, and Appendix A are submitted as Supplementary Information. Supplementary Information is available at www.ias.ac.in/chemsci.

Acknowledgements

P J is thankful to MHRD, Govt. of India for a fellowship under Technical Education Quality Improvement Program (TEQIP-II). Financial support to H S B and V R M from the Department of Atomic Energy (DAE), Govt. of India is

gratefully acknowledged. The authors are thankful to Dr. R. K. Behera of National Institute of Technology (NIT), Rourkela for NMR measurements and to Prof. Gautam K. Lahiri, Indian Institute of Technology, Mumbai for ESR measurement.

References

1. Kar A K, Acharya A N, Pradhan G C and Dash A C 2014 Glyoxylate as a reducing agent for manganese(III) in salen scaffold: A Kinetics and Mechanistic study *J. Chem. Sci.* **126** 547
2. Kar A K, Acharya A N, Mundlapati V R, Pradhan G C, Biswal H S and Dash A C 2014 Ligand substitution and electron transfer reactions of *trans*-(diaqua)(salen)manganese(III) with oxalate: an experimental and computational study *RSC Adv.* **4** 58867
3. Huynh M H V and Meyer T J 2007 Proton-coupled electron transfer *Chem. Rev.* **107** 5004
4. Lane B G 1994 Oxalate, germin and the extracellular matrix of higher plants *FASEB J.* **8** 294
5. (a) Sugiura M, Yamamura H, Hirano K, Sasaki M, Morikawa M and Tsuboi M 1979 Purification and properties of Oxalate Oxidase from Barley Seedlings *Chem. Pharm. Bull.* **27** 2003; (b) Aguilar C, Urzua U, Koenig C and Vicuna R 1999 Oxalate Oxidase from Ceriporiopsis subvermispora: biochemical and cytochemical studies *Arch. Biochem. Biophys.* **366** 275
6. Koyama H 1988 Purification and characterization of Oxalate Oxidase from pseudomonas Sp. Ox-53 *Agri. Biol. Chem.* **52** 743
7. Yuan M, Zhao F, Zhang W, Wang Z-Ming and Gao S 2007 Azide–bridged one-dimensional Mn^{III} polymers: effects of side group of schiff base ligands on structure and magnetism *Inorg. Chem.* **46** 11235
8. Ciringh Y, Gordon-Wylie Scott W, Norman R E, Clark G R, Weintraub S T and Horwitz C P 1997 Multinuclear paramagnetic NMR spectra and solid state X-ray crystallographic characterization of manganese(III) Schiff-base complexes *Inorg. Chem.* **36** 4968
9. Bonadies J A, Maroney M J and Pecoraro V L 1989 Structurally diverse manganese(III) Schiff base complexes: solution speciation via paramagnetic proton NMR spectroscopy and electrochemistry *Inorg. Chem.* **28** 2044
10. Sawyer D T and Roberts Jr. J L 1974 *Experimental Electrochemistry for Chemists* (New York: Wiley-Intersc.) p. 42
11. Perrin D D and Dempsey B 1974 *Buffers for pH and Metal Ion control* (London: Chapman and Hall) p. 120
12. Irving H M, Miles M G and Pettit L D 1967 A study of some problems in determining the stoichiometric proton dissociation constants of complexes by potentiometric titrations using a glass electrode *Anal. Chim. Acta* **38** 475
13. Mcgravey B R 1966 In *Transition Metal Chemistry*, R L Carlin (Ed.) (New York: Marcel Dekker Inc.) Vol. 3 p. 89
14. Jones T J and Noyes R M 1983 Mechanistic details of the oxidation of oxalate by Manganese(III) *J. Phys. Chem.* **87** 4686
15. Kovács B, Vizvári B, Riedel M and Tóth J 2004 Decomposition of the permanganate/oxalic acid overall reaction to elementary steps on integer programming theory *Phys. Chem. Chem. Phys.* **6** 1236
16. Alrichs R, Bär M, Häser M, Horn H and Kölmel C 1989 Electronic Structure Calculations on Workstation computers: The program system turbomole *Chem. Phys. Lett.* **162** 165
17. Treutlor O and Ahlrichs R 1995 Efficient molecular numerical integration schemes *J. Chem. Phys.* **102** 346
18. Vahtras O, Almlöf J and Feyereisen M W 1993 Integral approximation for LCAO-SCF Calculations *Chem. Phys. Lett.* **213** 514
19. Eichkorn K, Treutlor O, Öhm H, Häser M and Alrichs R 1995 Auxiliary basis sets to approximate coulomb potentials *Chem. Phys. Lett.* **240** 283
20. Eichkorn K, Treutlor O, Öhm H, Häser M and Alrichs R 1995 Auxiliary basis sets to approximate coulomb potential *Chem. Phys. Lett.* **242** 652
21. Fukuda T, Sakamoto F, Sato M, Nakano Y, Tan X Shi and Fujii Y 1998 Photopromoted oxidative cyclization of an o-phenylene-bridged Schiff base via manganese(III) complex, leading to fluorescent compound, 2-(2-hydroxyphenyl)benzimidazole *Chem. Commun.* 1391
22. McAuliffe C A, Nabhan A, Pritchard R G, Watkinson M, Bermejo M and Sousa A 1994 $[Mn(Salphen)(EtOH)_2](BH_4)$ [$SalphenH_2$ = *N*, *N″*-bis(salicylidene)-1,2-diaminobenzene], a further example of photosyntheic model compound forming dimers linked by hydrogen and π bonds *Acta Cryst. C* **50** 1676
23. Requena L and Bornemann S 1999 Barley (Horeum vulgare) oxalate oxidase is a manganese-containing enzyme *Biochem. J.* **343** 185
24. Opaleye O, Rose R-Sarah, Whittaker M M, Woo E J, Whittaker J W and Pickersgill R W 2006 Structural and spectroscopic studies shed light on the mechanism of oxalate oxidase *J. Biol. Chem.* **281** 6428
25. Noritke Y, Umezawa N, Kato N and Higuchi T 2013 Manganese Salen complexes with acid-base catalytic auxiliary: Functional mimetics of catalase *Inorg. Chem.* **52** 3653
26. Lanza V and Vechhio G 2009 New Conjugates of Superoxide dismutases/Catalases mimetics with cyclodextrins *J. Inorg. Biochem.* **102** 381
27. Olivera V and Vecchio G 2011 A novel artificial superoxide dismutase: Non covalent conjugation of albumin with a Mn^{III}-Salophen type complex *Eur. J. Med. Chem.* **46** 961
28. Liu Shih-Yuan, Soper J D, Yang J Y, Rybak-Akimova E V and Nocera D G 2006 Mechanistic Studies of Hangman Salophen-mediated activation of O–O bonds *Inorg. Chem.* **45** 7572
29. Riley D P 1999 Functional mimics of Superoxide Dismutase Enzymes as Therapeutic Agents *Chem. Rev.* **99** 2573
30. (a) Dahiya T and Pundir C S 2013 In vivo oxalate degradation by liposome encapsulated oxalate oxidase in rat model of hyperoxaluria *Indian J. Med. Res.* **137** 136; (b)

Gibson M I, Chen P Yang-Ting, Johnson A C, Piera E, Can M, Ragsdale S W and Drennan C L 2016 One Carbon Chemistry of Oxalate Oxidoreductase Captured by X-ray Crystallography *PNAS* **113** 320, and references cited therein

31. Signorella S, Palopoli C and Ledesma G 2018 Rationally designed mimics for antioxidant manganoenzymes: Role of structural features in the quest for catalysts with catalase and superoxide dismutase activity *Coord. Chem. Rev.* **365** 75